GLOBAL Scientific Inc. CHEMXPRESS

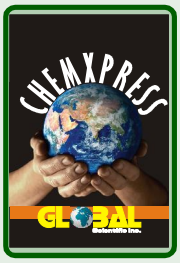

ORIGINAL ARTICLE

Structure, electrical and dielectric properties of praseodymium modified lead potassium niobate ceramic

T.Swarna Latha
Lecturer, PSC & KVSC Government Degree College, Nandyal, Kurnool district, Andhra Pradesh state, (INDIA)
E-mail: swasudha_phdau@yahoo.com
Received: 7th January, 2013 ; Accepted: 8th February, 2013

Abstract: Praseodymium modified Lead Potassium Niobate ($Pb_{1-x}K_{2x-3y}M_yNb_2O_6$ for x = 0.20, y = 0.10 and M =Pr) ferroelectric ceramic has been prepared by a high temperature solid state reaction technique. X-ray diffraction studies of the material at room temperature revealed orthorhombic structure with lattice parameters (a=17.715^{0}A, b= 17.973^{0}A, c=3.889 ^{0}A). The grain size of the sample has been found to be 4.46μm by using Scanning Electron Microscopy (SEM). Detailed dielectric study of sintered pellets as a function of temperature at different frequencies (500Hz, 1 KHz, 10 KHz, 20 KHz) and Curie temperature is found to be 340^{0}C. The impedance plots are used as tool to analyze the sample behavior as a function of frequency. The electrical process in the sample has been modeled in the form of an electrical equivalent circuit made up of a series combination of two parallel RC circuits attributed grains and grain boundaries. The Cole-Cole plots (Z' versus Z'') of impedance were drawn at different temperatures and showed non-Debye type relaxation. Modulus analysis reveals the possibility of hopping mechanism for electrical transport process in the systems. D.C and A.C conductivities of the sample as a function of temperature (from room temperature (RT) - 590^{0}C) have been studied. The frequency dependant ac conductivity at different temperatures showed the conduction process is thermally activated process.

Keywords: XRD; SEM; Dielectric; Impedance; Electric modulus; Conductivity.

ORIGINAL ARTICLE

INTRODUCTION

Ferroelectric oxides of tungsten bronze (TB) ferroelectric family are a class of important materials for applications in various electronic devices such as multilayer capacitors, transducers, actuators, ferroelectric random access memory and display, microwave dielectric resonators, pyroelectric detector, and so forth, owing to their unique electro-optic, non linear optic, photo refractive index, pyroelectric effect, and acoustic optic properties[1-7]. The TB structure has a general chemical formula $[(A_1)_2(A_2)_4(C)_4][(B_1)_2(B_2)_8]O_{30}$, where the A site usually filled by divalent or trivalent cations, and the B sites by Ta^{5+}, V^{5+} or Nb^{5+} atoms. This structure consists of an arrangement of corner sharing BO_6 octahedrons forming three interstitial sites. The smallest interstice C site is empty, so the general formula can be $A_6B_{10}O_{30}$ for filled TB structure. There is a scope for variety of cationic substitutions at the interstitial sites (i.e., A_1, A_2, B_1, B_2) that can tailor the physical properties of the materials for device applications[8]. One of the most known of these compounds is the lead potassium niobate with general formula $Pb_{1-x}K_{2x}Nb_2O_6$ (PKN)[9], when rare earth ions doping then this formula have been reduces to $Pb_{1-4x}K_{2x}M^{3+}{}_{2y}Nb_2O_6$ (M=rare-earth=Pr) and derived compounds. The PKN has a large electromechanical coupling factor of bulk waves, surface acoustic wave (SAW)'s and a small temperature coefficient of small fundamental frequencies, which was first discovered by Yamada and et al.[10-13].

Impedance spectroscopy has been widely used for investigating the properties of electric materials and electrochemistry systems. No report has been found on the studies, dielectric, impedance, and conductivity properties on ceramics of praseodymium doped lead potassium niobate $Pb_{0.8}K_{0.1}Pr_{0.1}Nb_2O_6$ (Pr-PKN). Present paper describes preparation, structure, dielectric, impedance, modulus and conductivity studies on Pr - PKN ceramic.

EXPERIMENTAL

A mixed high temperature solid-state reaction oxide method was used for the preparation of Pr-PKN ceramic:

$$0.80(PbO) + 0.05(K_2CO_3) + 0.05(Pr_2O_3) + Nb_2O_5 \rightarrow Pb_{0.8}K_{0.1}Pr_{0.1}Nb_2O_6 + 0.05CO_2$$

Required amount of AR-grade powders of PbO, K_2CO_3, Pr_2O_3 and Nb_2O_5 have been taken to yield Pr – PKN compound grounded well in agate mortar in methanol medium and calcined at 900^0C/4h. The calcination procedure has been repeated three times to achieve homogeneous with single phase composition. The calcined powder is then mixed with required amount of poly vinyl alcohol as a binder. The powder obtained was compacted under hydraulic press with 580 Mpa pressure and made into pellets of 12mm in diameter and 2mm in thickness. Then the pellets are placed on a platinum foil and the calcined powder was sprinkled on the surface of the sample to compensate the loss of lead. The assembly was closed with an inverted crucible then sintered at 1165^0C for 1 hour. The sample has been glass polished and electroded with conducting silver paste on both surfaces. The microstructure on the specimens of present compound was obtained with a scanning electron microscopy SEM, JEOL, JSM – 5400. The lattice parameters were estimated using the interpretation and indexing School of physical sciences, Flinders University of south Australia, Bedford Park, Australia. The dielectric constant and impedance measurements were performed on the material (from room temperature (RT) to 600^0C) in frequency range 45Hz - 5MHz using computer interfaced HIOKI 3532-50 LCR HiTESER.

RESULTS AND DISCUSSION

Structure

Figure 1 shows the X-ray diffractogram on the material of praseodymium doped lead potassium niobate $Pb_{0.8}K_{0.1}Pr_{0.1}Nb_2O_6$ (Pr-PKN). The calcined powder has been taken for X-ray diffraction studies (2θ=10-90^0) using CuK_α radiation. All the peaks have been indexed by using an interactive powder diffraction data interpretation and indexing program revealing the material has single phase with orthorhombic structure. The lattice parameters a, b and c are calculated. The 100% intensity peak in $Pb_{1-x}K_{2x}Nb_2O_6$ (PKN) with x = 0.20 has been reported at $2\theta = 32^O\ 223'$[9] which is found to be the characteristic feature of the composition. The

ORIGINAL ARTICLE

same has been fpund to be at30^0 068'. The shift in due to the substitution of praseodymium. The substitution of Pr^{3+} in PKN reduces the lattice parameters of PKN (a=17.723 Å, b=17.987 Å, c=3.895 Å[14]) to a=17.715 Å, b=17.973 Å and c=3.889 Å. The experimental density (d_{exp}) has been found to be 77.5% to that of the theoretical value (d_{the}) in the materials Pr-PKN. The values of lattice parameters, orthorhombic distortion (b/a), d_{the}, d_{exp}, porosity and %density have been given in TABLE 1.

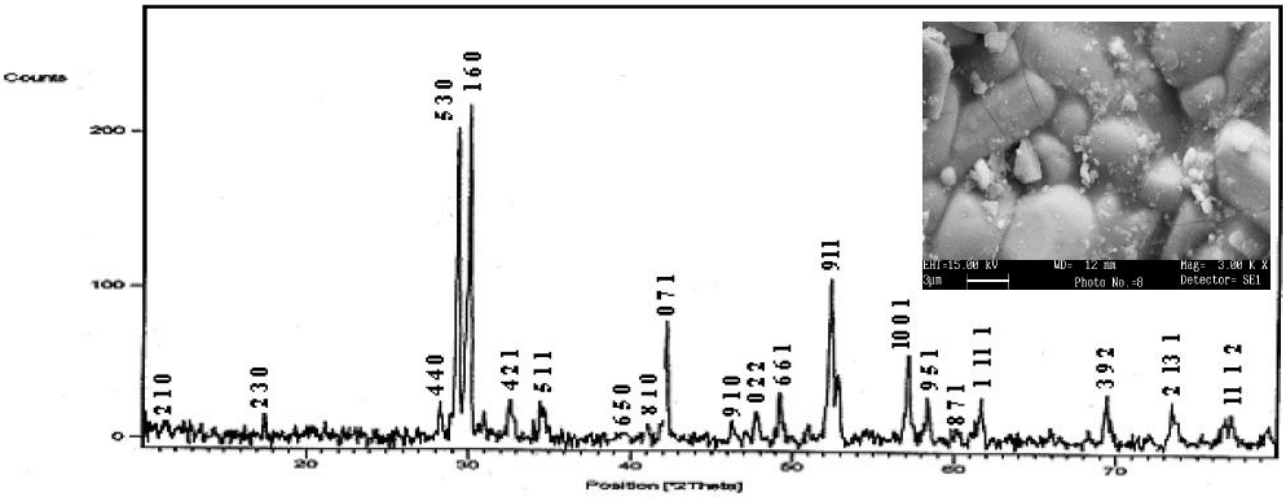

Figure 1 : X–ray diffractogram of Pr-PKN. (Inset. SEM micrograph of $Pb_{0.8}K_{0.1}Pr_{0.1}Nb_2O_6$).

TABLE 1 : Lattice parameters of Pr-PKN.

Composition	Lattice Parameters(Å)	Cell volume(Å^3)	Orthorhombic Distortion(b/a)	Density(g/cm^3)		Porosity	Density (%)
	a=17.715Å			d_{the}	d_{exp}		
Pr-PKN	b=17.973Å	1238.22	1.014	6.24	4.84	0.22	77.56
	c=3.889 Å						

Temperature and frequency dependence of dielectric constant

Variation of real (ε') and imaginary part of dielectric constant (ε'') with temperature (from room temperature to 600^{0}C) at 500Hz, 1KHz, 10KHz and 20KHz have been shown in Figure 2(a,b). The values of ε' and ε'' increase with decreasing frequency, which is the characteristic feature of polar dielectric materials. A maximum of real dielectric constant (ε') related to the paraelectric-ferroelectric transition (T_c,°C), which is observed at 340°C which is much lower than that of PKN (T_c=500°C)[9].

This may be due to the ferroelectric phase transition for TB structure compounds possessing not only displacive characteristic but also order disorder characteristics[15]. Also, ionic size polarizability and electronic configuration of the ions participating in solid solution are believed to be among the factors that determine the magnitude and direction of the shift of T_c. The T_c is sharp and fits to the Curie-Weiss law (ε=C/T-θ) in Para region. The curie constant has been found to be 0.6x10^5 K, which is the characteristic of oxygen octahedra ferroelectrics[16,17]. Further, the T_c is found to be the same for different frequencies. It indicates that Pr: PKN belongs to traditional ferroelectric but not relaxor. The peak values of the real dielectric constant (ε'_{Tc}) and room temperature dielectric constant (ε'_{RT}) have been found to be 1124.3 and 148.2 respectively at the frequency 1KHz.

Inset of Figure 1 shows the SEM micrograph of Pr:PKN. It is clear from the figure that the grains are clearly visible, indicating the existence of polycrystalline microstructure. Linear intercept method has been used to determine the average grain size in present composition. The value of grain size is 4.46 µm.

From Figure 2(b), a shift in the value of (ε'') has been observed at a particular temperature 340^{0}C. The temperature at which shift is observed exactly coincides with the value of T_c. This again confirms that the material is traditional ferroelectric. The shift has been showed in inset figure (c) at frequency 10 KHz.

ORIGINAL ARTICLE

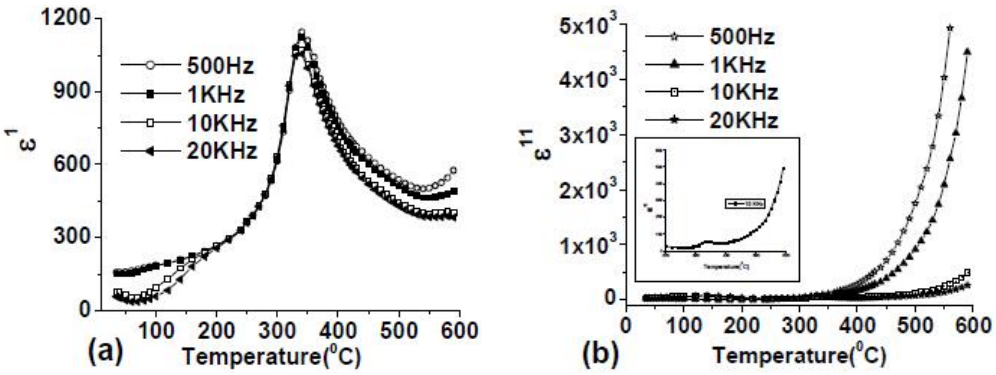

Figure 2 : Variation of (a, b) real and imaginary parts of the dielectric constant with temperature.

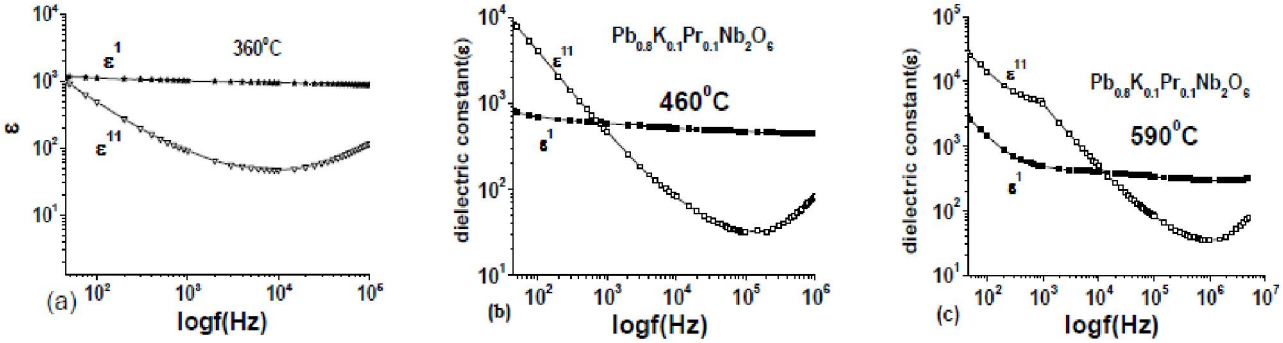

Figure 3(a,b,c) : Frequency dependence of real and imaginary parts of the dielectric constant, ε^1 and ε^{11} at various temperatures.

Figure 3(a-c) shows the variation of real and imaginary parts of dielectric constants, ε' and ε'', as a function of frequency at various temperatures (360^{0}C, 460^{0}C and 590^{0}C). At 360^{0}C and 45Hz, ε' and ε'' shows 1174 and 992 respectively and both intersect at 75Hz. As temperature increased to 460^{0}C the intersection frequency shifts to the higher side at 800Hz. On further increasing in temperature to 590^{0}C the intersecting frequency shifts to 15 KHz. Both ε' and ε'' rise sharply towards low frequencies and the shape of rise is changed as the temperature increases. ε' and ε'', exhibits high value which reflects the effect of space charge polarization and/or conducting ionic motion. As it is known, in the conducting dielectric materials, high ε' values may be related to the accumulation of charges at the interface between the sample and electrodes, i.e., space charge polarization. Corresponding, ε'' of the low frequency become very high due to free charge motion within the material and are connected to ac conductivity relaxation.

IMPEDANCE ANALYSIS

Figure 4(a,b) shows the variation of the real ($Z^{'}$) and imaginary ($Z^{''}$) part of impedance with frequency at several temperatures (300^{0}C to 590^{0}C). From Figure 4(a) It is observed that the magnitude of $Z^{'}$ & $Z^{''}$ decreases with the increase in both frequency as well as temperature, and all curves are merge at high frequencies for all temperatures above 10^4 Hz. This may be due to the release of space charges. From Figure 4(b), the curves show that the $Z^{''}$ values reach a maxima peak ($Z^{''}_{max}$) for the temperatures e"380°c. This indicates the single relaxation process in the system. The curves display decrease in $Z^{'}$ with temperature and indicate an increase in a.c. conductivity with temperature and frequency (i.e. negative temperature coefficient of resistance behaviour like that of semiconductor). For the temperature below 380°c, the peak was beyond the range of frequency measurement. The value of Z''_{max} and corresponding frequency for the maximum f_p shifts to higher frequencies with increasing temperature, indicating the increasing loss in the sample. The peak heights are proportional to bulk resistance (R_b) according to equation in Z" Vs frequency plots $Z^{11} = R_b[-\omega\tau/(1+\omega^2\tau^2)]$[18].

Figure 5 shows the normalized imaginary parts,

ORIGINAL ARTICLE

Z''/Z''_{max}, of the impedance as a function of frequency on 0.2Pr:PKN at several temperatures. The Z''/Z''_{max} parameter exhibits a peak with a slightly asymmetric degree at each temperature especially at higher temperatures; it seems that high temperature triggers another relaxation process. At the peak, the relaxation is defined by the condition $\omega_m\tau_m=1$, $\tau_{m=}$ relaxation time. The asymmetric broadening of the peaks suggests the presence of electrical processes in the material with a spread of relaxation time. The relaxation species in the material may possibly be immobile species /electrons at low temperatures and defects/vacancies at higher temperatures. The relaxation frequency obeys the Arrhenius relation given by $\omega_m=\omega_0 \exp[-E\tau/K_BT]$, where ω_0 is a pre-exponential factor. The activation energy E_τ is calculated from the ω_m -1/T plots (Figure 6). The calculated activation energy in the Para region (440^0C-595^0C) is 0.60 ev.

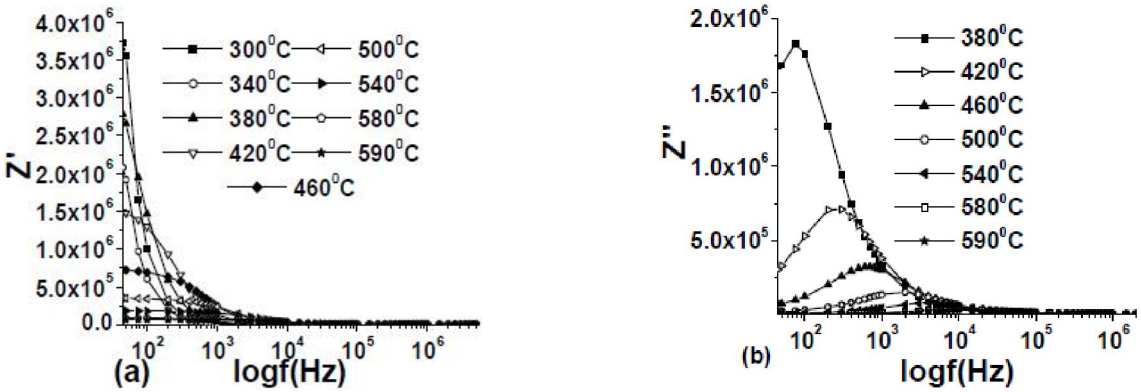

Figure 4 : (a) Variation of real part of impedance with frequency at different temperatures; (b) Variation of imaginary part of impedance with frequency at different temperatures.

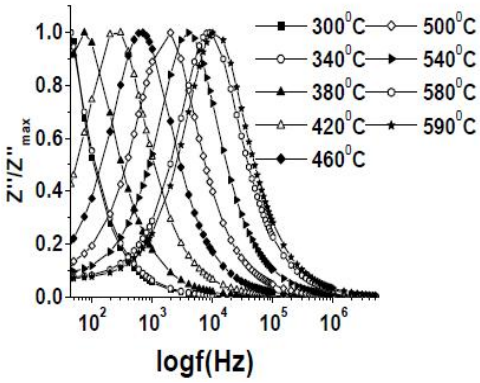

Figure 5 : Normalized imaginary part of impedance Z''/Z''_{max}.

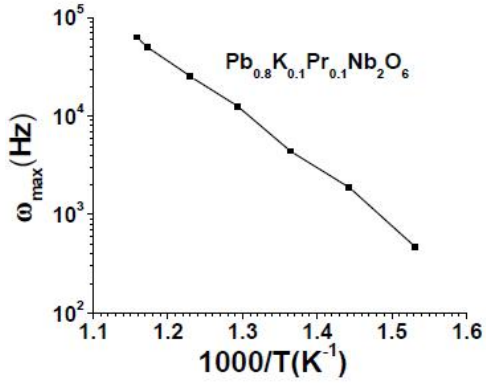

Figure 6 : Temperature dependence of relaxation as function of frequency at several temperatures.

Figure 7(a) shows the frequency dependence of Z' and Z'' at 580^0C. As the frequency increases Z'' increases whereas Z' decreases. This trend continues up to a particular frequency which Z'' occupies a maximum value and Z' intersects, further increase in frequency, both Z' and Z'' decreases, and above 10 KHz both the values merges with X-axis. This indicates there exits a relaxation phenomenon. Figure 7(b) shows Argand diagram (imaginary part of complex impedance Z^* versus its real part) allows the determination of bulk ohmic resistance as a function of temperature and thus temperature dependence of conductivity.

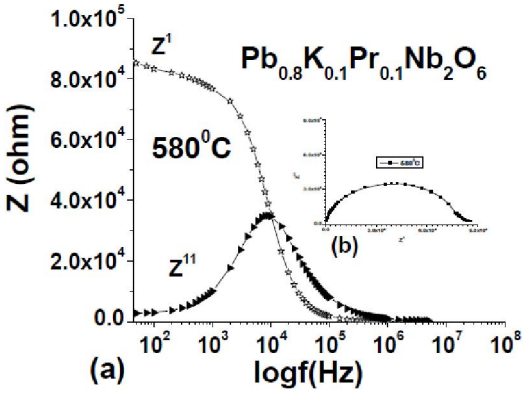

Figure 7 : (a) Frequency dependence of Z^1 and Z^{11} and (b) corresponding Argand diagram.

ORIGINAL ARTICLE

Complex impedance formalism helps in determining inter-particle interaction like grain, grain boundary effects, etc. To study the contribution due to different effects, Cole-Cole analyses have been done at different temperatures. It also provides information about the nature of dielectric relaxation. For pure mono-dispersive Debye process, one expects semicircular plots with the centre located on the Z' – axis whereas, for poly-dispersive relaxation, these argand plane plots are close to circular arcs with endpoints on the axis of real and the centre below this axis. The complex impedance in such situations is known to be described by Cole-Cole formalism[19]. $Z^*(\omega) = Z' + iZ'' = R / [1 + (i\omega / \omega_o)^{1-\alpha}]$, where α represents the magnitude of the departure of the electrical response from an ideal condition and this can be determined from the location of the centre of the Cole-Cole circles. When α goes to zero ($1-\alpha \rightarrow 1$), the above equation gives rise to classical Debye's formalism. Figure 8 shows a set of impedance data taken over a wide frequency range (45Hz-5MHz) at several temperatures as a Nyquist diagram. At lower temperature (<300^{0}C) there is a linear response in Z[11]. This trend indicates the insulating behavior in the Pr-PKN sample. As the temperature increases above300^{0}C the linear response gradually changes to semicircle in nature. At and above 420^{0}C the single arc found in the sample can be resolved into two semicircles with overlapping. These semicircles can be represented by the equivalent two parallel RC elements which are in series[20,21]. Figure 9. Shows the equivalent circuit. These semicircles start from origin. Hence there is no series resistance that can be attached to the equivalent RC circuit.

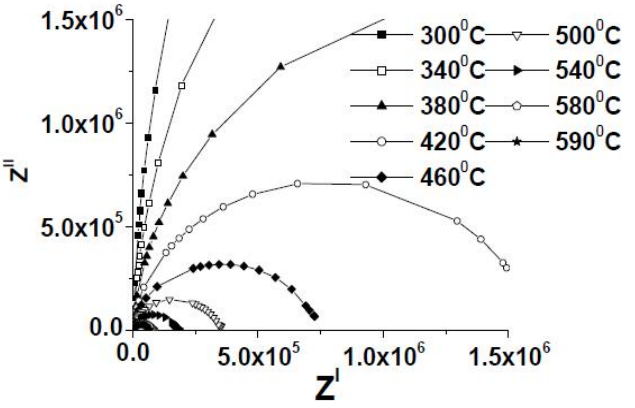

Figure 8 : Nyquist diagram.

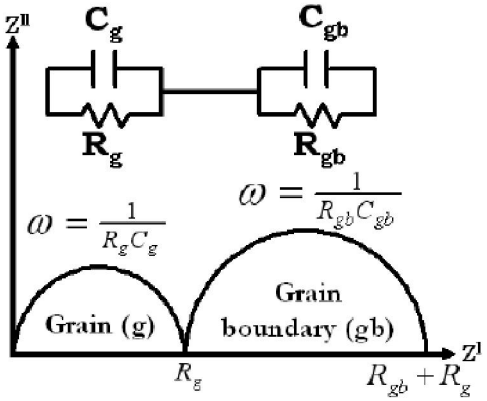

Figure 9 : Equivalent circuit.

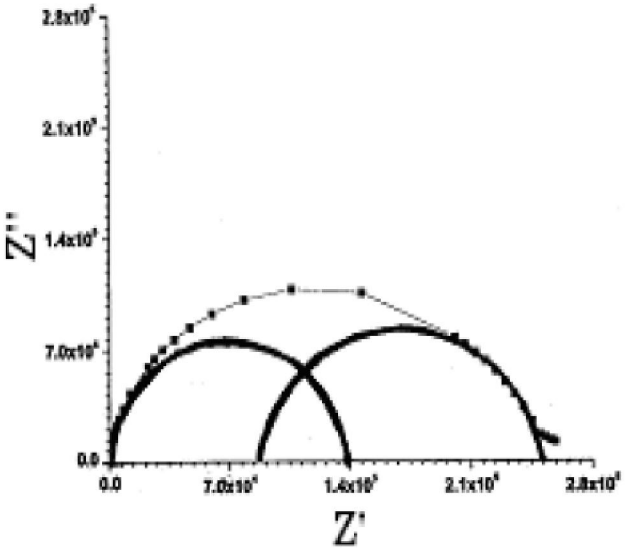

Figure 10 : Cole-cole plot at different temperatures 520^{0}C.

Figure 10 Shows that the Cole-Cole plot for T = 520^{O}C. From the temperature 420^{O}C these semicircles are resolved into two semicircular arcs having its centers lying below the real axis. The semicircular arcs appear in distinct frequency ranges (one at a higher frequency followed by another lower frequency semicircular arc) as shown in (Figure 10). The resistance of bulk (R_b), grain boundary (R_{gb}) could directly be obtained from the intercept on the Z'-axis. The circular fitting of the semicircular arcs in the impedance spectrum gives a measure of the grain and grain boundary resistance as well as relaxation time following equation $\omega\tau = 2\pi f_{max} RC = 1 \Rightarrow f_{max} = 1/2\pi RC$ and $\tau = 1/2\pi f_{max}$ Where f_{max} is the frequency of the maximum of semicircles.

Figure 11(a to c) shows variation of R_g, R_{gb}, C_g, C_{gb}, τ_g, τ_{gb} with temperature. It is evident from Figure 12(a). As the temperature increases the R_{gb} is found to be less than R_g. From Figure11(b), it could be ob-

ORIGINAL ARTICLE

served that, at 420^{0}C both grain and grain boundary capacitance have same value of 1.96nF. But from 440^{0}C temperature the C_g value is greater than C_{gb} value. From Figure 11(c) It could be observed that $\tau_g > \tau_{gb}$. The activation energy values of grain and grain boundary due to conduction and relaxations are 0.43 ev, 0.38 ev and 0.58 ev, 0.45 ev respectively, i.e., in the present compound it appears that the conduction is mainly through the grain rather than grain boundaries.

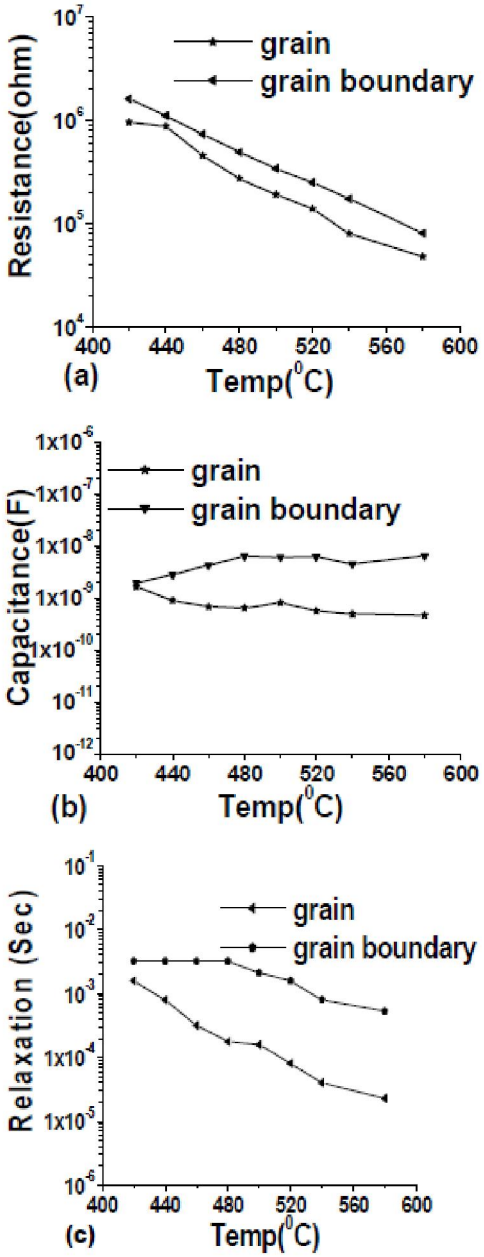

Figure 11(a,b,c) : Variation of resistance, capacitance and relaxation time of grain and grain boundary with temperature.

MODULUS SPECTROSCOPY

From the physical point of view, the electrical modulus corresponds to the relaxation of the electrical field in the material when the electric displacement remains constant. Therefore, the modulus represents the real dielectric relaxation process[22]. The usefulness of the modulus representation in the analysis of relaxation properties was demonstrated both for ionic conductors[23] and polycrystalline ceramics[24]. In practice, regions of low capacitance, such as grain interiors, are characterized using M" data, whereas more resistive regions, such as grain boundaries and pellet surface layers, which often have higher associated capacitance, are characterized using Z" spectra[25].

The complex electrical modulus is parameters that can be expressed as a Fourier transform function φ (t) that gives the time evolution of the electric field within the dielectric,

$$\varepsilon^* = \varepsilon^1 - i\varepsilon^{11}$$

$$M^*(\omega) = 1/\varepsilon^* = M'(\omega) + i\,M''(\omega)$$

$$= M_{\infty}[-+''\exp(-i\omega t)(d\Phi(t)dt)dt]$$

$$= (\varepsilon^1 + i\varepsilon^{11})/\varepsilon^{1^2} + \varepsilon^{11^2}$$

The variation of the real and imaginary parts of the electrical modulus with frequency (45Hz-5MHz) at various temperatures (300^{0}C -590^{0}C). From Figure12(a), at low frequency region as temperature increases the magnitude of M' decreases. The value of M' observed to be constant below 340^{0}C at all the frequencies. Above 340^{0}C, from 1 KHz, the value of M' appears to be increased sharply, confirming the presence of an appreciable electrode and/or ionic polarization in temperature studied[26]. From Figure 12(b), the temperature beyond 420^{0}C, the value of M" increases to a peak at a particular frequency and it is appears to be shifting towards higher frequency side as the temperature increases. The trend in M" continues. However, the value of M" at 45 Hz decreases with increase in temperature. M" spectra are broadened on the high frequency side. It is obvious that the low frequency side of the peak represents the range of frequencies in which the ions can move over long distances i.e., ions can perform successful hopping from one site to the neighboring site. The high frequency side of M" peak represents the range of

ORIGINAL ARTICLE

frequencies in which the ions are spatially confirmed to their potential wells and the ions can make only localized motion within the wells[27,28]. The peak of M" represents the relaxation angular frequency (ω_p) and is satisfying the Arrhenius behavior.

Figure 13 Shows the Arrhenius plot of relaxational angular frequency ω_p ($\omega 0 \exp [-E_\mu/K_B T]$) as a function of inverse of temperature and the activation energy is found to be 0.50 ev.

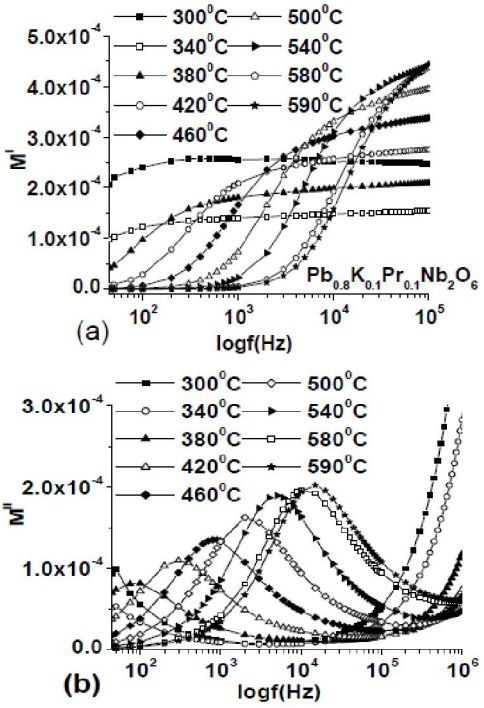

Figure 12 : (a) Variation of real part of electric modulus(M') with frequency and (b) Variation of imaginary part of electric modulus (M") with frequency.

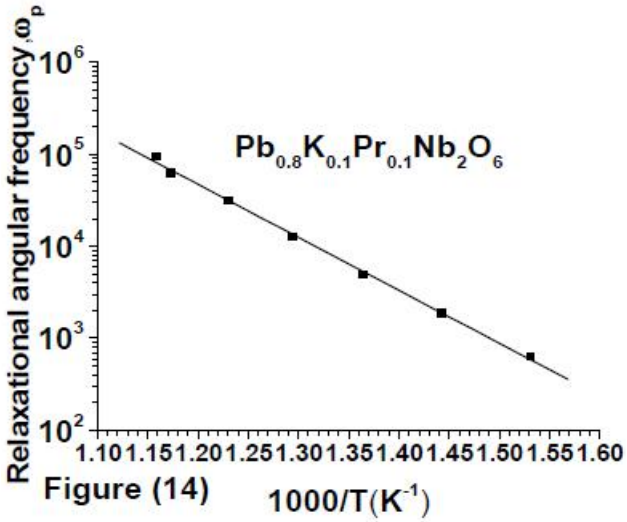

Figure 13 : Arrhenius plot of relaxation frequency obtained from M" peaks as a function of 1/T.

CONDUCTIVITY ANALYSIS

From Figure 14(a) the electrical conductivity, σ (ω) as a function of frequency at different temperatures (260°C to 590°C). The conductivity depends on frequency according to the 'universal dynamic response' for ionic conductors[29] given by the phenomenological law $\sigma(\omega) = \sigma_{d.c} + A\omega^n$. Where A is a thermally activated quantity and n is the frequency exponent and can take the value 0<n< 1. The switch from the frequency independent $\sigma_{d.c}$ to the dependent σ (ω) regions shows the onset of the conductivity relaxation phenomenon and the translation from long range hopping to the short range ion motion[30]. The dispersion in conductivity at low frequencies may be due to the electrode polarization.

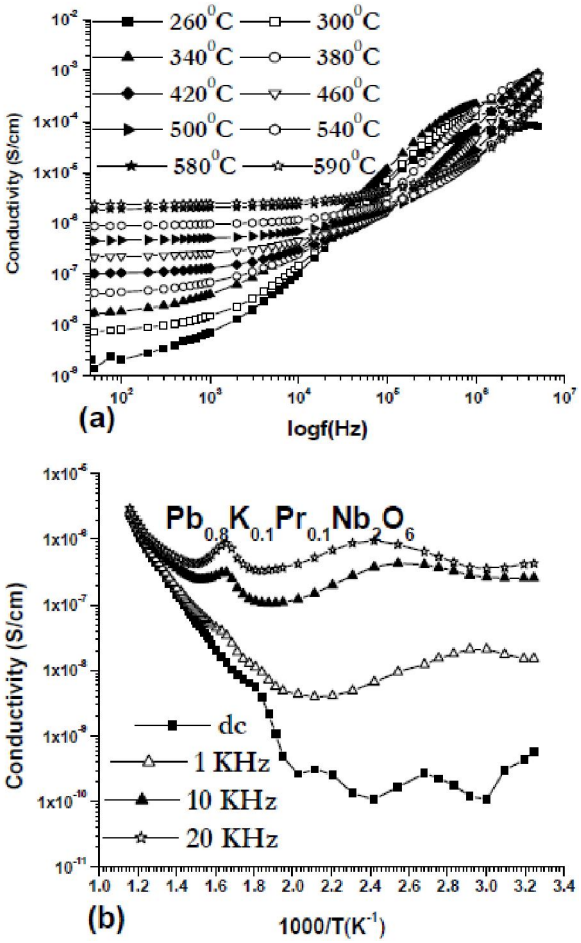

Figure 14(a) : Frequency dependence of real part of AC conductivity at various temperatures; (b) AC conductivity as a function if inverse temperature at various frequencies.

From Figure14(b) the a.c conductivity of the sample depends on the dielectric nature of the sample.

ORIGINAL ARTICLE

The $\sigma_{a.c}$ is plotted against $10^3/T$ at various frequencies. The non appreciable variation of $\sigma_{a.c}$ with temperature indicates the multiple relaxations. The a.c conductivity process is dependent on the capacitance of the sample. The dispersion at lower temperature possibly indicates the presence of space charge of the material that vanishes at higher frequency and temperatures. The frequency variation of $\sigma_{a.c}$ involves a power exponent (ω^n, n is the exponent and ω is angular frequency of a.c field). This indicates that the conduction process is a thermally activated process. From the graphs it is seen that the exponent as depicted by the slope of the variation is a function of temperature

The activation energy values in the system were calculated from the slope of the graphs (Figure 15 b) of Arrhenius plots of the conductivity as a function of inverse temperature for three regions are given in TABLE 2.

TABLE 2 : Activation energy values of $\sigma_{a.c}$ is plotted against $10^3/T$ at various frequencies.

Temperature range (^{0}C)	Activation energy (ev)			
	20 kHz	10 KHz	1 KHz	d.c
260-330	0.37	0.37	0.37	0.41
395-500	0.14	0.21	0.34	0.45
510-590	0.10	0.47	0.22	0.24

CONCLUSIONS

1. XRD analysis of $Pb_{0.8}K_{0.1}Pr_{0.1}Nb_2O_6$ ceramic confirmed the single phase with orthorhombic structure with lattice parameters a=17.715 Å, b=17.973 Å and c=3.889 Å. The T_c of the compound has been found to be 340^{0}C, and belongs to classical ferroelectrics.
2. It is observed that ε' and ε" intersecting only from 360^{0}C in low frequency range. There is sharp raise in ε' and ε" towards low frequency (45 Hz) side may be due to conducting ion motion. High value of ε' may be interpreted as accumulation of charge at interface between sample and electrode i.e., space charge polarization.
3. The appearance of two semicircles in the Cole-Cole plots (at 420^{0}C) reveals that there are two relaxations mechanisms due to grain and grain boundary.
4. The Z" peaks are shifted towards higher frequency side, and peak heights are decreased with increase in temperature, which reveals an increase in the relaxation in the systems. The M" peak frequencies increase with increase in temperature. This shift of the M" peaks correspond to the so-called conductivity relaxation.
5. It is observed that the activation energies obtained from impedance, modulus and conductivity studies at 1 KHz in ferro region is typical values for ionic conductors.
6. Thermal behavior of AC conductivity showed change in slope at T_C and found to merge at higher temperatures due to onset of intrinsic conductivity.

REFERENCES

[1] R.J.Xie, Y.Akimune, R.P.Wang, K.Matsuo, T.Sugiyama, N.Hiro Saki; J.Amer.Ceram.Soc., **85**, 2725-2730 **(2002)**.
[2] C.Huang, A.S.Bhalla, R.Guo, Article ID 211907, **86(21)**, 3 **(2005)**.
[3] Y.Yuan, X.M.Chen, Y.J.Wu; J.Appl.Phys., Article ID 084110, **98(8)**, 5 **(2005)**.
[4] M.R.Ranga Raju, R.N.P.Choudary, H.R.Rukmini, Ferroelectrics, **325**, 25-32 **(2005)**.
[5] J.H.Kko, S.Kojima, S.G.Lushnikov, R.S.Katiyar, T.H.Kim, J.H.Ro; J.Appl.Phys, **92,(3)**, 1536-1543 **(2002)**.
[6] M.Lee, R.S.Feigelson, A.Liv, L.Hesselink; J.Appl.Phys., **83(11)**, 5967-5972 **(1998)**.
[7] K.S.Rao, T.N.V.K.V.Prasad, N.Vallisnath, V.R.K.Murthy; Botswana Journal of Technology, **12(2)**, 1-7 **(2003)**.
[8] Banarji Behera, P.Nayak, R.N.P.Choudhary; J.Alloys and Comp.
[9] K.S.Rao, P.M.Krishna, T.Swarnalatha, D.M.Prasad; Mat.Sci.Engg.B, **131**, 127 **(2006)**.
[10] T.Yamada; J.Appl.Phys., **46**, 2894 **(1975)**.
[11] T.Yamada; J.Appl.Phys.Lett., **23**, 213 **(1973)**.
[12] H.Yamauchi; Appl.Phys.Lett., **32**, 599 **(1978)**.
[13] J.Nakano, T.Yamada; J.Appl.Phys., **46**, 2361 **(1975)**.
[14] P.Jana, R.K.Pandey, B.W.Donnely; Presented at IMF8, **(1993)**.
[15] X.M.Zheng, X.M.Chen; J.Mater.Res., **17**, 1664 **(2002)**.
[16] K.S.Rao, A.S.V.Subramanyam, S.Murali Mohan

Rao; Ferroelectrics, **109**, 771 **(1997)**.
[17] T.R.Shrout, L.E.Cross, D.A.Hukin; Ferroelectr. Lett., **44**, 325 **(1983)**.
[18] R.V.Hipple; Dielectrics and waves, NY: John Wiley and Sons, **(1954)**.
[19] K.S.Cole, R.H.Cole; J.Chem.Phys., **9**, 341 **(1941)**.
[20] I.M.Hodge, M.D.Ingram, A.R.West; J.Ame.Cer. Soc., **74**, 125 **(1976)**.
[21] R.P.Tandon; J.Kor.Phys.Soc., **32**, 327 **(1998)**.
[22] H.Wagner, R.Richert; Polymer., **38**, 5801 **(1997)**.
[23] P.B.Macdo, C.T.Moynihan, R.Bose; Phys.Chem. Glasses, **13**, 171 **(1972)**.
[24] J.Liu, Ch.G.Duan, W.G.Yin, W.N.Mei, R.W.Smith, J.R.Harday; J.Chem.Phys., **119**, 2812 **(2003)**.
[25] N.Hirose, A.R.West; J.Am.Ceram.Soc., **79**, 1633 **(1996)**.
[26] J.S.Kim, T.K.Song; J.Phys.Soc.Japan, **70**, 3419 **(2001)**.
[27] P.Pissis, A.Kyritsis; Solid state ionics, **97**, 105 **(1997)**.
[28] R.L.Ngai, C.Leon; Solid state ionics, **125**, 81 **(1999)**.
[29] J.Grigas; Microwave dielectric spectroscopy of ferroelectrics and related materials, Gordon and Breach Publishing Inc., Amsterdam, **(1996)**.
[30] R.Mizaras, M.Takashige, J.Banys, S.Kojima, J.Grigas, Hamazaki, Sin-Ichi, A.Brilingas; J.Phys.Soc.Jpn., **66**, 2881 **(1997)**.